Paper

Mechanism of High Grain Refinement Effectiveness on New Grain Refiner "TiBAl Advance" *

Akihiro Minagawa** and Matthew Piper***

Grain refiners are used in the aluminum DC casting process to refine the cast structure. On the other hand, high levels of TiB_2 particles and other inclusions from the grain refiner can cause clogging of the melt filter. Improvement of the grain refinement effectiveness is required in order to reduce the addition level of grain refiners. The grain refiner manufacturer AMG developed "TiBAl Advance", which is a high performance Al-3Ti-1B (mass%, following is same) grain refiner. TiBAl Advance has passed a special casting test to provide grain refiners with a high grain refinement efficiency. However, the reason why it shows such high grain refinement effectiveness is yet to be clarified. In this work, the grain refinement effectiveness of TiBAl Advance was compared to that of conventional grain refiners. In addition, the TiB_2 agglomerate size distributions were measured in each refiner and applied to the new UACJ model for grain size prediction. TiBAl Advance was demonstrated to have superior grain refinement effectiveness compared with other conventional grain refiners. Furthermore, the predicted grain size from the new UACJ model agreed well with the experimental results. Based on these results, it was estimated that the superior grain refinement effectiveness of TiBAl Advance is due to the smaller size of TiB_2 agglomerates, and consequently greater number of heterogeneous nuclei available for any given volume fraction of TiB_2.

Keywords: *Aluminum, DC casting, Grain refiner, Grain refinement, Boride, Agglomerate*

1. Introduction

In aluminum DC casting processes, grain refinement is necessary to promote a fine, equiaxed grain structure, which reduces the risk of casting defects such as hot tears[1), 2)]. It is commonplace to use grain refiner alloy additions as a convenient means of obtaining the desired grain structure. Typical grain refiners are based on the Al-Ti-B system, and contain TiB_2 and Al_3Ti particles. Al_3Ti particles dissolve after addition, contributing to the solute titanium content. Although an effective grain refinement particle, excessive additions of TiB_2 particles (and other inclusions associated with grain refiners) can cause clogging of the melt filter[3)]. In order to reduce the necessary addition levels of grain refiner, an improvement in the grain refinement effectiveness is required. The grain refiner manufacturer AMG Aluminum has developed "TiBAl Advance", which is a high-performance Al-3Ti-1B grain refiner. TiBAl Advance has passed a special, proprietary casting test to guarantee a high grain refinement efficiency – meaning that, despite lower addition rates, finer grain sizes can be realized. However, the fundamental reason why it demonstrates such high grain refinement effectiveness still requires clarification.

Many investigations concerning the mechanism of grain refinement have been reported[4)~12)]. Maxwell and Hellawell developed a numerical approach to predict grain size[4)]. They concluded that the number of nucleation events depends on recalescence under isothermal conditions. Greer et al. proposed a free growth model based on that of Maxwell and Hellawell[5), 6)]. This model defined the initiation of free growth of grains on an inoculated particle by undercooling of melt, and is well-known by those in the industry because of its accuracy in the prediction of grain sizes. However, even with the free growth

* The main part of this paper has been published in Light Metals 2021, ed. by L. Perander, (2021), 844-849.

** Research Department Ⅱ, Research & Development Division, UACJ Corporation

*** AMG Aluminum

model, the differences between more or less efficient refiners cannot be explained[6]. More recently, it has been suggested that the size and distribution of TiB_2 agglomerates, rather than individual particles, is the cause of different grain refinement efficiencies[13), 14)], however, this aspect has not been applied to the grain size prediction model.

In this study, the mechanism of high grain refinement effectiveness of TiBAl Advance was explored via comparison with conventional grain refiners. In addition, TiB_2 agglomerate size distributions were measured in each refiner, the results of which were applied to the new UACJ model for grain size prediction.

2. Experimental method

The grain refinement efficiency of four grain refiner samples was investigated. **Table 1** shows the sample list of grain refiner. The grain refinement effectiveness was evaluated using the AA TP1 test. In this study, amount of melt was reduced to 5 kg to improve workability. (AA TP1 standard is 10 kg.) Other aspects of the test method followed the AA TP1 standard. **Table 2** describes the casting conditions. Addition levels of grain refiner were 0.1, 0.07, 0.05 and 0.03 % for each grain refiner. These tests were carried out in 99.7 % purity aluminum. The chemical content of the base aluminum (before addition of grain refiner) was determined by spark optical emission spectroscopic analysis and is shown as C_0 in **Table 3**. 5 kg of base aluminum was melted by an electric furnace and maintained in the range of 713-723 ℃ . The grain refiner was added to the molten aluminum, and stirred for 30 seconds by graphite stick. In addition, the molten aluminum was again stirred for 15 seconds before taking cast samples. The cast samples were taken by a conical steel ladle 10 minutes after the grain refiner addition. The ladle was removed to the cooling equipment and quenched from bottom. The cooling rate at the observation position of microstructure was 6.4 K/s. The cross section at a position 38 mm from the ingot bottom was polished. The microstructures were observed by an optical microscope. The average grain size was measured by the planimetric method.

Table 1 Sample list of grain refiner.

Sample name	Manufacturer	Chemical content (mass%)
TiBAl Advance	AMG	Al-3Ti-1B
AMG 5/1	AMG	Al-5Ti-1B
B 3/1	B	Al-3Ti-1B
B 5/1	B	Al-5Ti-1B

Table 2 Casting conditions.

Parameters	Values	Unit
Grain refiner	4	type
Addition level of grain refiner	0.03, 0.05, 0.07, 0.1	%
Base aluminum	99.7	%
Amount of melt	5	kg
Melt temperature	991	K
Holding time	10	min
Cooling rate	6.4	K/s

Table 3 Chemical content of base aluminum (mass%).

Solute element	Fe	Si	V	Ti
C_0	0.10	0.03	0.02	0.005

3. Grain size prediction model

A UACJ prediction model for grain size is based on the free growth model[5]. Part of the equation was modified from the free growth model to take into account the liquidus slope m, the equilibrium partition coefficient k and initial content C_0 for all solute elements. The free growth of a crystal on a TiB_2 particle depends on the undercooling ΔT_{fg}. The undercooling ΔT_{fg} required to start the free growth is given by

$$\Delta T_{fg} = \frac{2\sigma}{\Delta S_V r^*} \quad (1)$$

where ΔS_V is the entropy of fusion per unit, σ is the solid-liquid interfacial energy, and r^* is the critical embryo radius. The overall melt undercooling ΔT is the sum of the solute undercooling ΔT_s and the curvature undercooling ΔT_c. The solute undercooling ΔT_s is given by

$$\Delta T_s = m\left(C_0 - C_{IL}\right) \quad (2)$$

where C_{IL} is the solute content in the liquid at the solid-liquid interface. C_0 is the solute content in the melt. The curvature undercooling ΔT_c is given by

$$\Delta T_c = \frac{2\sigma}{\Delta S_V r} \quad (3)$$

where r is the radius of the spherical crystal. The invariant-size approximation model[15] was proposed for the diffusion controlled growth of a spherical precipitate of radius in a solid matrix. According to the model, the radius of a spherical particle is given by

$$r = \lambda (D \cdot t)^{1/2} \quad (4)$$

and differentiating eq.4 with respect to time gives the growth rate of the spherical crystals as

$$V = \frac{dr}{dt} = \frac{\lambda^2 D}{2r} \quad (5)$$

where D is the solute diffusion coefficient in the liquid and t is the time. λ is an interfacial parameter and obtained from the interface composition profiles[15] as

$$\lambda = \left(\frac{-S}{2\pi^{1/2}}\right) + \left(\frac{S^2}{4\pi} - S\right)^{1/2} \quad (6)$$

in which

$$S = \frac{2(C_{IL} - C_0)}{(C_{IS} - C_{IL})} \quad (7)$$

where C_{IS} is the solute content in the solid at the solid-liquid interface. S can vary between-2 and 0[4]. Substituting Eq.2 and the equilibrium partition coefficient $k = C_{IS}/C_{IL}$, Eq.7 becomes

$$S = -2 \cdot \frac{\Delta T_S}{m(k-1)(C_0 - \Delta T_S/m)} \quad (8)$$

The value of one element can be used for parameters like m, k and C_0 in case of Eq.8. Therefore, Eq.8 has been modified to consider alloys including numerous elements. In most cases, ΔT_s is very small with TiB_2 particle and ΔT_s/m can be ignored. Consequently, Eq.8 becomes

$$S \approx -2 \cdot \frac{\Delta T_S}{mC_0(k-1)} = -2\,\frac{\Delta T_S}{Q} \quad (9)$$

in which

$$Q = mC_0(k-1) \quad (10)$$

where Q is termed the growth-restriction parameter. By using parameter Q, it is possible to consider m and k for all solute content, regardless of element. Furthermore, where ΔT_s is very small (< 1 K) and Q values are an order of magnitude larger than ΔT. That means |S| << 1 and Eq.6 simplified to

$$\lambda \approx (-S)^{1/2} = \left(2\frac{\Delta T_S}{Q}\right)^{1/2} = \left(\frac{2(\Delta T - \Delta T_C)}{Q}\right)^{1/2} \quad (11)$$

The calculation process is the same as that of the free growth model. The temperature decreases at each time step according to the set cooling rate. Each grain will grow at the rate calculated by Eq.5 if the total undercooling ΔT reaches or exceeds ΔT_{fg}. In this study, the TiB_2 agglomerate radius was treated as r^* in Eq.1, because the TiB_2 agglomerate were assumed to act as a heterogeneous nuclei. The rising temperature, which is the total latent heat divided by the specific heat, was added to the next time step. **Tables 4 and 5** show the physical property values and the solute element parameters used in calculations, respectively. The soluble titanium from the grain refiner was calculated, according to the addition level, and added to the initial titanium content.

In this study, TiB_2 agglomerate size distributions were applied to the model. Longitudinal cross sections of the grain refiners were polished. In order to measure the TiB_2 agglomerate size, the polished surface was deep etched by 5 mass% NaOH aqueous solution for 15 minutes. The etched surface of the samples was observed by SEM. The observed points were near surface of the rod and center of diameter.

Table 4 The material parameters used in the calculation[5].

Physical property	Symbol	Units	Value
Solid-liquid interfacial energy	σ	J/m²	158×10^{-3}
Entropy of fusion per unit volume	ΔS_V	J/(K m³)	1.112×10^6
Enthalpy of fusion per unit volume	ΔH_V	J/m³	9.5×10^8
Heat capacity of melt per unit volume	C_{PV}	J/(K m³)	2.58×10^6
Diffusivity in melt (Ti in Al)	D	m²/s	2.52×10^{-9}

4 samples were taken at each position, giving a total of 8 SEM images for every sample. The TiB_2 agglomerate sizes were measured as equivalent diameter of projected area by imageJ software[16].

4. Results

The results of the AA TP1 test are shown in **Fig. 1**. The grain refinement effectiveness of TiBAl Advance surpassed that of the conventional grain refiners at all addition rates. Conversely, the grain refinement effectiveness of "B 3/1" was poor, especially at the 0.03 % addition level. In these test conditions it was found that the grain size achieved with "B 5/1" at the refiner addition of 0.1 % could be achieved with 0.05 % refiner addition level by using TiBAl Advance.

Fig. 2 shows the cumulative frequency distributions of TiB_2 agglomerates, as revealed by the deep etch technique in the grain refiner microstructures. The horizontal axis represents the equivalent diameter of projected area of TiB_2 agglomerate, with the vertical axis representing the cumulative frequency of volume. The graph shows that TiBAl Advance has a distribution of generally smaller TiB_2 agglomerates compared with other grain refiners. These distributions were applied to the UACJ prediction model to calculate the number of TiB_2 agglomerates by size classification. A comparison of grain size between experiments and calculations is shown in **Fig. 3**. By considering the TiB_2 agglomerates as heterogeneous nuclei, the predicted values are in good agreement with the experimental results.

Table 5 The solute element parameters used in the calculation[5].

Solute element	m/K・s^{-1}	k/−
Fe	−2.925	0.03
Si	−6.62	0.12
V	9.71	3.33
Ti	25.63	7

5. Discussion

Good prediction accuracy was obtained by consideration of the TiB_2 agglomerate size distribution, providing confirmation that larger TiB_2 agglomerates act as a heterogeneous nuclei prior to smaller ones. However, in the case that the grain

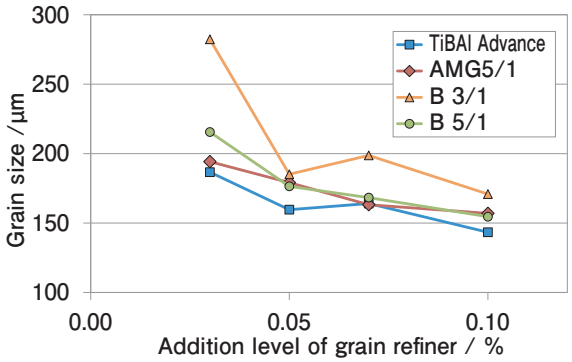

Fig. 1 Grain refinement test results.

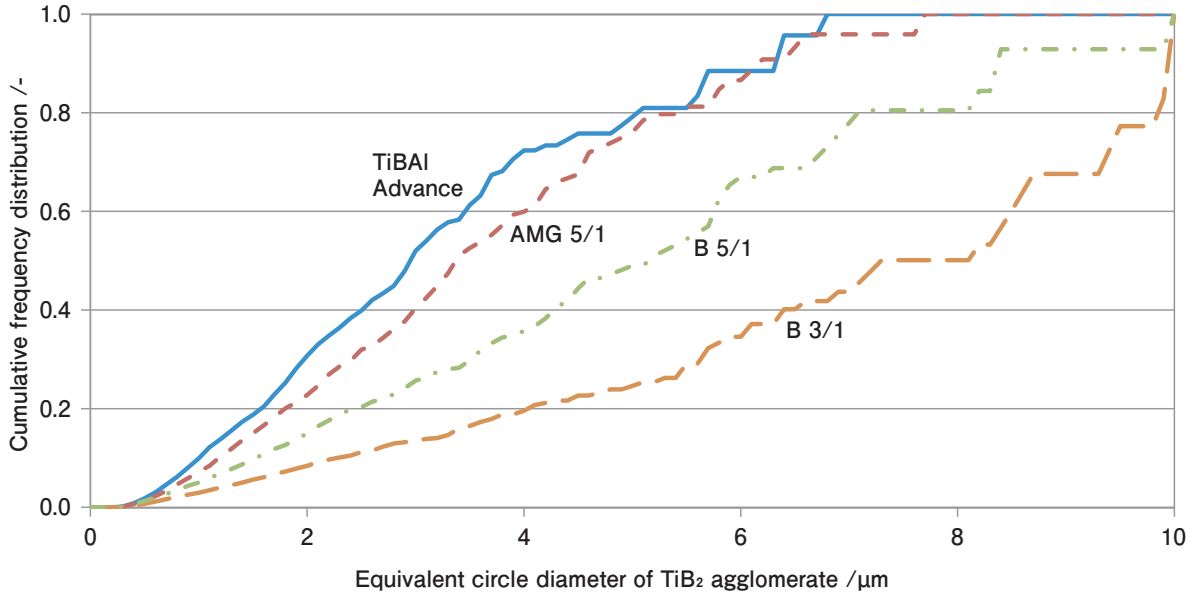

Fig. 2 Cumulative frequency distribution of TiB_2 agglomerate.

refiner contains larger TiB_2 agglomerates, the total number of TiB_2 agglomerates must decrease, given a constant volume fraction of TiB_2. Consequently, it is considered that the grain refinement effectiveness of "B 3/1" and "B 5/1" was observed to be comparatively less at lower addition rates, due to fewer available heterogeneous nuclei.

There are few reports of the heterogeneous nuclei detected in the cast sample[17]. In order to validate the model, it is necessary to confirm the presence of the TiB_2 agglomerates, in or near to the center of grains in the cast samples. Therefore, the cast samples with the target addition level of 0.1 % were observed using SEM. These samples were deep etched in 5 mass% NaOH aqueous solution for 15 min before observation to facilitate easier detection of the TiB_2 agglomerates. **Fig. 4** shows an example of the observation, where a TiB_2 agglomerate in the center of a grain was observed. The number of the observed TiB_2 agglomerates was five or more in each cast sample. The equivalent circle diameters, (based on the projected area) of the observed TiB_2 agglomerates were measured. **Fig. 5** shows the comparison between the measured values and the predicted values of TiB_2 agglomerate diameters, for each grain refiner type. The predicted value is the average diameter of TiB_2 agglomerate predicted to initiate nucleation, determined by the agglomerate size distributions from Fig. 2 and calculated by the model. The predicted value and measured value show good agreement. From these results, it is estimated that TiB_2 agglomerates can act as heterogeneous nuclei, thus providing validation for the model. Therefore, it is suggested that the high grain refinement effectiveness of TiBAl Advance grain refiner is due to the smaller size of TiB_2 agglomerates, and consequently a greater number of heterogeneous nuclei available for any given volume fraction of TiB_2. In order to confirm whether the TiB_2 agglomerates acted as heterogeneous nuclei, future investigation into the crystal orientations between TiB_2 agglomerates and aluminum grains is required.

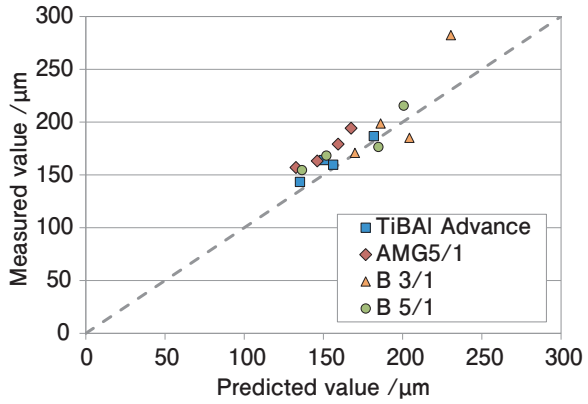

Fig. 3 Comparison of grain size between experiment and calculations.

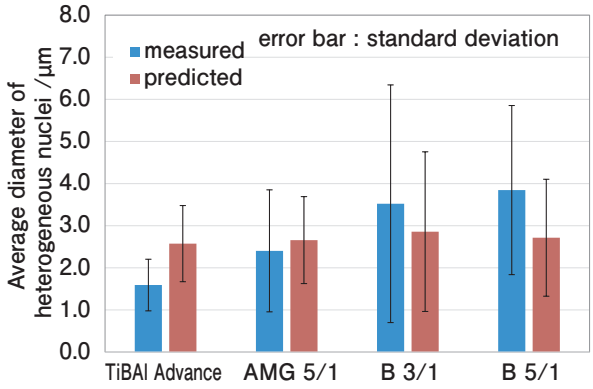

Fig. 5 Comparison of TiB_2 agglomerate size between measured value and predicted value.

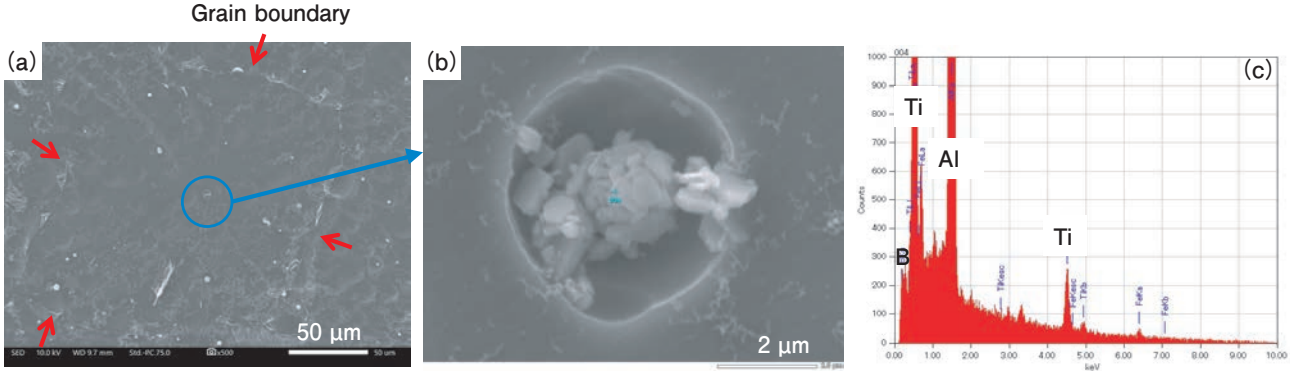

Fig. 4 (a) SEM image of a grain. Red arrow indicates the grain boundary, (b) SEM image of TiB_2 agglomerate. (c) The result of content analysis by EDS.

6. Conclusion

1. TiBAl Advance showed a high grain refinement effectiveness, which can be exploited to reduce addition levels of grain refiners in the casthouse.
2. The average TiB_2 agglomerate size in TiBAl Advance was smaller when compared with that of the conventional grain refiners.
3. The experimental and predicted grain sizes were in good agreement when the TiB_2 agglomerate size distribution was applied to the prediction model.
4. The size of the observed TiB_2 agglomerates in or near to the center of grains showed good agreement between measured and predicted values.
5. From these results, it was suggested that "TiBAl Advance" shows high grain refinement effectiveness due to the smaller size of TiB_2 agglomerates, and consequently greater number of heterogeneous nuclei available for any given volume fraction of TiB_2.
6. The UACJ prediction model was proved to be valid and useful.

Acknowledgment

This is a post-peer-review, pre-copyedit version of an article published in Light Metals 2021. The final version is available online at: https://doi.org/10.1007/978-3-030-65396-5_111.

REFERENCES

1) D. G. Eskin, Suyitno and L. Katgerman: Prog. Mater. Sci., **49** (2004), 629-711.
2) S. Li, K. Sadayappan and D. Apelian: Metall. Mater. Trans. B, **44** (2013), 614-623.
3) C. Voigt, B. Fankhänel, B. Dietrich, E. Storti, M. Badowski, M. Gorshunova, G. Wolf, M. Stelter and C. G. Aneziris: Metall. Mater. Trans. B, **51** (2020), 2371-2380.
4) I. Maxwell and A. Hellawell: Acta Metall., **23** (1975), 229-237.
5) A. L. Greer, A. M. Bunn, A. Tronche, P. V. Evans and D. J. Bristow: Acta Mater., **48** (2000), 2823-2835.
6) A. M. Bunn, P. V. Evans, D. J. Bristow and A. L. Greer: Light Metals 1998 (1998), 963-968.
7) D. H. StJohn, M. Qian, M. A. Easton and P. Cao: Acta Mater., **59** (2011), 4907-4921.
8) M. A. Easton and D. H. StJohn: Mater. Sci. Eng. A, **486** (2008), 8-13.
9) M. Qian, P. Cao, M. A. Easton, S. D. McDonald and D. H. StJohn: Acta Mater., **58** (2010), 3262-3270.
10) W. Dai, X. Wang, W. Zhao and Q. Han: Light Metals 2014, (2014), 945-949.
11) R. Vainik, L. Backerud and J. Courtenay: Light Metals 2006, (2006), 789-791.
12) A. Prasad, S. D. McDonald, H. Yasuda, K. Nogita and D. H. StJohn: J. Cryst. Growth, **430** (2015), 122-137.
13) A. Minagawa: Light Metals 2020, (2020), 988-993.
14) G. Salloum-Abou-Jaoude, P. Jarry, P. Celle and E. Sarrazin: Light Metals 2020, (2020), 994-999.
15) H. B. Aaron, D. Fainstein and G. R. Kotler: J. Appl. Phys., **41** (1970), 4404-4410.
16) C. A. Schneider, W. S. Rasband and K. W. Eliceiri: Nature Methods, **9** (2012), 671-675.
17) S. Furuta, A. Minagawa, I. Matsui, Y. Murakami, N. Omura, A. Takeuchi, K. Uesugi and M. Kobayashi: Materialia, **10** (2020), 100663.

Akihiro Minagawa
Research Department Ⅱ,
Research & Development Division,
UACJ Corporation

Matthew Piper
AMG Aluminum